Atmospheric Emitted Radiance Interferometer Part II: Water Vapor and Atmospheric Aerosols

B.A. Whitney, H.E. Revercomb, R.O. Knuteson, F.A. Best, and W.L. Smith
University of Wisconsin - Madison
Madison, Wisconsin

Introduction

Atmospheric Emitted Radiance Interferometer (AERI) spectra provide detailed characterization of the infrared component of the surface radiation budget (Ellingson et al. 1995), support spectroscopic (Clough et al. 1989; Revercomb et al. 1995) and cloud (Smith et al. 1992; Collard et al. 1995) radiative modeling studies for improving radiative transfer calculations, and are the basis for high time-resolution remote sensing of atmospheric state parameters (Feltz et al. 1996). Here we focus on the quantification of sources of opacity in the clear sky window region, one of the key spectroscopic issues for accurate surface energy budget modeling. Three important contributors to uncertainty in the window region opacity that are somewhat difficult to separate are 1) water vapor continuum, 2) aerosols, and 3) atmospheric water vapor profile. We present progress in investigations of the latter two contributors, which we expect will ultimately lead to refinements in the water vapor continuum. New information has better defined the uncertainties of atmospheric water vapor observations, and approaches for reducing these uncertainties are being formulated and tested.

Regarding aerosols, last year we reported evidence that the spectral signature of a typical rural aerosol is present in a large number of the AERI spectra from the Southern Great Plains (SGP) Atmospheric Radiation Measurement (ARM) Program site (Revercomb et al. 1995). Subsequently we learned that the smallest signatures identified as aerosols with large visibilities were actually caused by a small obstruction to the prototype AERI's sky view (see AERI Part I, Revercomb et al. 1996). We present revised estimates of aerosol effects using corrected AERI prototype data. The peak effects are not significantly changed, but the percentage of spectra identifiably affected is significantly lower.

Evidence for Problems in Observing Atmospheric Water Vapor

The SGP data sets indicate significant inconsistencies in the atmospheric water vapor observed by radiosondes (Balloon-Borne Sounding System [BBSS]), the Surface Meteorological Observing System (SMOS), the 60-m tower, and the microwave sounder. Fortunately, the data sets themselves are now becoming sufficiently extensive to help reveal which observations need improvement. Here we demonstrate that comparisons of properties derived from radiation observations with those from in situ radiosonde observations provide a mechanism to identify the sources of inconsistencies. One quantity of interest is the difference between AERI-observed radiances and the Line-By-Line Radiative Transfer Model (LBLRTM; Clough and Iacono 1995; Clough et al. 1995) calculated radiances from the AERI/LBLRTM Quality Measurement Experiment (QME). These residuals, averaged over part of the long-wave window (800-1000 cm^{-1}), are shown in Figure 1 for a 21-month dataset taken at the Cloud and Radiation Testbed (CART) site. The sparse distribution of points with differences exceeding ~10 $mW/m^2/sr/cm^{-1}$ are probably caused by the effects of undetected clouds on AERI radiances. While the primary purpose of the AERI/LBLRTM residuals is to form the basis for improving radiative transfer models, for this discussion we are using the residuals to characterize relative errors in the radiosonde water vapor measurements that are used to define the atmospheric state for the model (LBLRTM). For example, if the radiosonde measures too much water, the model will produce higher radiance in the window region, and the AERI/LBLRTM difference will be smaller than it should be. Similarly, if the radiosonde measures too little water, AERI/LBLRTM is larger.

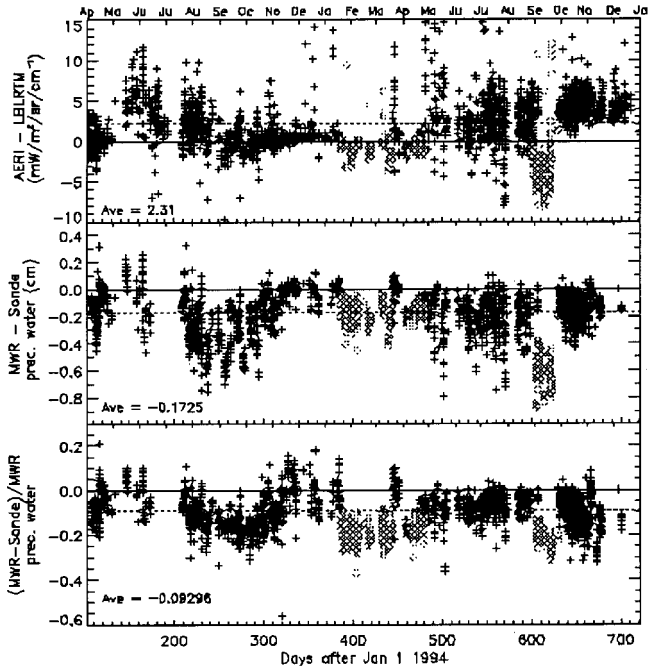

Figure 1. The top panel shows AERI/LBLRTM residuals averaged over 800-1000 cm^{-1} (10-12.5 microns) and plotted over a 21 month period beginning in April 1994. Since the model (LBLRTM) uses radiosonde measurements for its atmospheric state, a correlation between the AERI/LBLRTM difference and the microwave (MWR)/radiosonde difference (middle panel) indicates that the radiosonde varies in time. The bottom panel shows the fractional difference in total precipitable water measured by the MWR and radiosondes. The dotted lines are the 21-month averages. The light grey points are known to have sonde calibration errors (see text).

The middle panel of Figure 1 shows the difference between the microwave radiometer (MWR) and radiosonde measurements of total precipitable water during this same 21-month time range. These time-dependent differences are a direct indication of a measurement inconsistency, with the microwave being drier on the average by 1.7 mm or about 9%. The microwave precipitable water retrievals were tuned to 1992-1993 radiosonde averages, and may in the future be revised based on theoretical arguments to be independent of radiosonde measurements (Liljegren, private communication; see also Clough and Brown 1996). If the MWR measures accurately, or at least is stable over time, but the radiosonde has time-dependent errors, then the MWR-radiosonde precipitable water should be directly correlated with AERI/LBLRTM. On the other hand, if the MWR has variable errors, but the radiosondes are consistent, then any variations in AERI/LBLRTM should be uncorrelated with variations in MWR-radiosonde, since the MWR is not used in the AERI/LBLRTM calculation. The 1995 data shows a strong positive correlation between the top and middle panels. This correlation implies that there are indeed significant variations in radiosonde accuracy for this period. The bottom panel of Figure 1 reduces the seasonal bias on the MWR/radiosonde comparison by plotting fractional differences. The variations shown here imply a radiosonde error of 40% peak-to-peak, with a standard deviation of 7.8%.

One source of error in the radiosonde was recently discovered by B. Lesht (Lesht and Liljegren 1996), who identified a calibration batch dependence during 1995. The shaded circles in Figure 1 mark batches of radiosondes that were improperly calibrated for relative humidity. Eliminating the mean 7% wet bias of the bad batches (see bottom, Figure 1) would definitely improve the consistency of the data. However, the remaining differences are still large—the standard deviation of the remaining data points drops only to 7.2%—implying that efforts should be made to reduce sonde-to-sonde differences. Steps are being taken to provide more ground-based in situ observations (at the BBSS launch site and at the 25-m tower level to augment the current 60-m measurement) to help define sonde-to-sonde calibration differences.

Existing water vapor observations from the 60-m tower provide further information on the inconsistency of observations characterizing the atmospheric water vapor profile. Comparisons of tower and radiosonde observations at the 60-m level for October 1995 are shown in Figure 2. The period is especially interesting because it contains significant variations in the water vapor content (shown by the thin line in Figure 2), it followed shortly after the tower water vapor sensor was repaired and calibrated, and it did not include any of the bad radiosonde calibration batches. Note the large (±20%) diurnal variations of the sonde-tower differences. These differences warn that the direct use of tower observations to correct for sonde-to-sonde variations is dangerous. It has been shown by M. Wesely (personal communications) that tower-sonde differences are correlated with local atmospheric lapse rate, implying that these differences are related to the finite time constant of the radiosonde observations. Hopefully, having accurate ground-based measurements for comparison with the ventilated radiosonde measurements before launch, coupled with tower observations at both 25 and 60 m, will allow both the sonde lag and sonde-to-sonde calibration variations to be accounted for accurately.

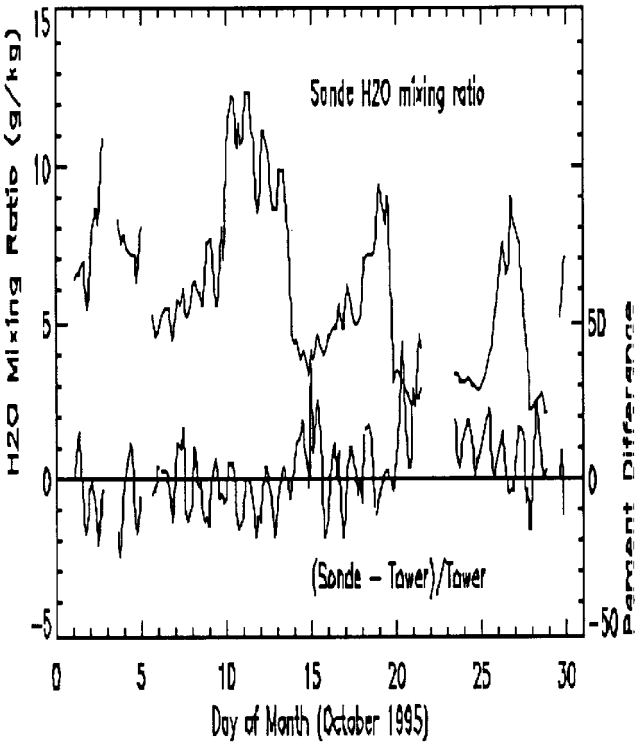

Figure 2. Water vapor mixing ratio measured by the radiosonde (thin line), and the percent difference between radiosonde and Tower (thick line) measurement at 60 meter height.

AERI Evidence for Raman Lidar Stability

The Raman lidar measurements of water vapor profiles provide a means to check and correct for inconsistencies in the radiosonde measurements. While the calibration of the lidar is based on radiosonde measurements, it appears to be stable in time compared to a set of radiosonde measurements. The Goddard Space Flight Center Raman Lidar operated during the April 1994 Intensive Observation Period (IOP) at the CART site. Table 1 shows all of the clear-sky observations that took place during the IOP when the AERI, radiosondes, and Raman lidar operated (the lidar operated only at night). The table entries are ordered in increasing precipitable water amount, as measured by the Raman Lidar. Figure 3 shows an example of the radiosonde and Raman water vapor profiles compared. Note that a constant scaling of the radiosonde agrees reasonably well with the Raman. We scaled the radiosonde to the Raman and attached the radiosonde profile at the bottom and top to provide a new profile. We then ran LBLRTM models on all of the observations shown in Table 1. Figure 4 shows the AERI/LBLRTM averaged longwave window-region difference, as in Figure 1, both with the original radiosonde profiles (plus signs) and the Raman profile (diamonds). It is clear from this plot that the Raman profile gives more consistent residuals. The standard deviation of this set of points drops from 1.7 $mW/m^2/sr/cm^{-1}$ using the radiosonde profiles to 0.6 using the Raman. The extremely high aerosol case of April 26, 1994, is not included in this set since the high residual is due to aerosol rather than water vapor error.

These results show that routine operation of the Sandia Raman Lidar at the SGP CART site can provide a basis to significantly reduce the large reproducibility errors in current sonde water vapor profiles (Figure 1). Then, it would be possible to achieve absolute accuracy in the atmospheric water vapor profiles, as needed for the AERI/LBLRTM QME, by making infrequent, highly accurate, water vapor observations to establish the absolute calibration of the Raman lidar, now based on radiosondes. The radiosonde would still be used for temperature and to define the profile below and above the Raman range. In addition, the Raman will operate continuously, including daytime, and therefore can provide water vapor profiles to make AERI/LBLRTM comparisons at times in between radiosonde launches.

Absolute Water Vapor Calibration and Water Line Spectroscopy from AERI: Approach and Progress

This section describes the use of on-line AERI data itself to help resolve absolute water vapor uncertainties. The basic idea is to first eliminate uncertainties related to effects giving low spectral resolution radiance contributions (e.g., continuum and aerosols) by creating an artificial model "continuum" that is tuned to match AERI observations. By matching the regions between lines, the on-line radiometric effect of low-resolution contributors will be properly accounted for, even if the modeled mechanisms for these effects are not understood. Then on-line differences uniquely represent spectroscopic or atmospheric water vapor uncertainties. By varying the modeled water profile by multiplicative constants from the measured radiosonde or Raman Lidar profiles (while holding the tuned "continuum" constant), the best fit for each water line of interest can be determined. Figure 5 (top) shows an example AERI-00 spectrum from 30 August 1995 during the CAMEX field program compared to four LBLRTM calculations using a radiosonde plus GSFC Raman lidar water vapor profile increased by 0, 10, 20, and 30% (and a fixed continuum chosen to fit between the lines). The percentage water vapor increase which best fits each of the five largest

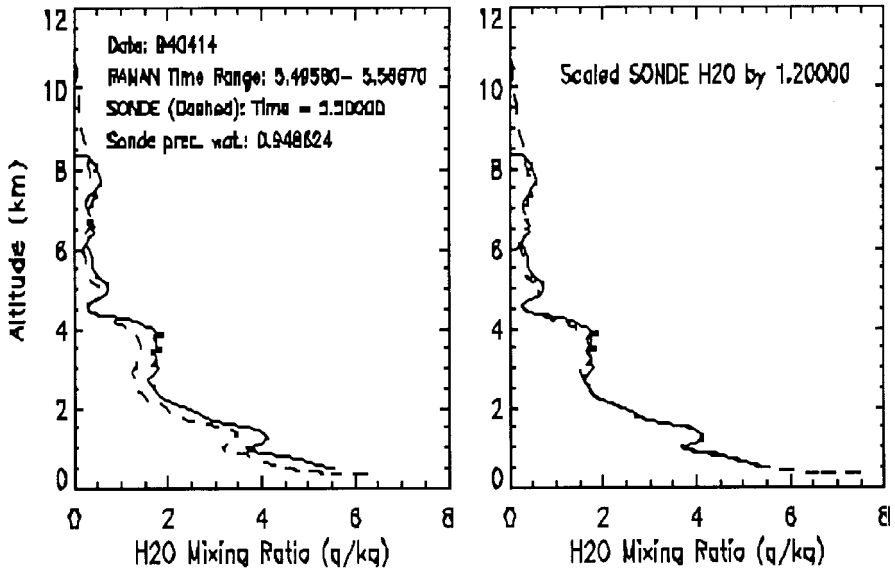

Figure 3. Comparison of Raman and radiosonde atmospheric water vapor profiles.

Table 1. Clear-sky observations during the IOP.

Date	Time	Integrated Precipitable Water			Aerosols		
		Raman	Sonde	MWr	Raman bsr[a]	AERI res.[b]	Model vis.[c]
940426	8.63	0.76	0.72	0.73	1.03	Y	40
940426	5.54	0.76	0.82	0.73	1.06	Y	23
940416	5.41	0.82	0.93		1.01	N	
940418	5.71	0.94	1.06	0.93	1.06	N	
940416	8.85	0.96	1.06		1.04	N	
940418	8.43	0.98	1.09	1.00	1.02	N	
940414	8.45	1.16	1.10		1.07	N	
940414	5.56	1.18	0.96		1.07	N	
940417	8.62	1.18	1.33		1.02	N	
940415	8.67	1.50	1.43		1.08	Maybe	40
940419	8.44	1.68	1.80	1.61	1.07	N	
940426	2.82	1.73	1.62	1.43	1.47	Y	4
940423	5.35	2.35	2.59	2.19	1.28	N	
940424	5.42	2.82	2.87	2.53	1.35	N	
940424	8.34	2.98	2.81	2.66	1.24	N	

(a) GSFC Raman backscatter ratio (ratio of aerosol to molecular scattering).
(b) A positive AERI-LBLRTM residual indicates a possible aerosol signature.
(c) Model visibility required to fit AERI-LBLRTM residual.

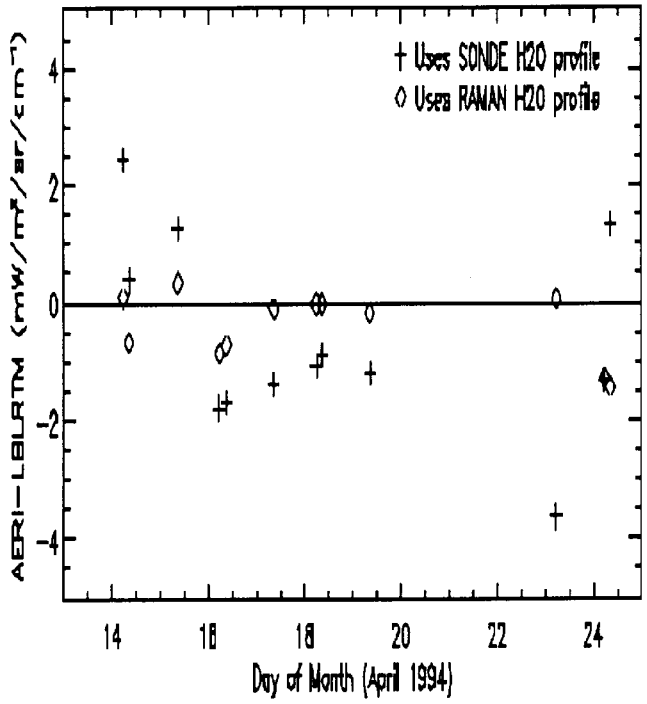

Figure 4. Comparison of AERI/LBLRTM residuals averaged over 800-1000 cm^{-1}, using radiosonde (pluses) and Raman (diamonds) water vapor profiles as input to LBLRTM.

spectral lines in the top panel is shown in the bottom panel of Figure 5 for four observations, including three from the Remote Cloud Sensing IOP at the SGP Site in April 1994 and one from Wallops Island, VA, on 30 August 1995. At this point, the stated spectroscopic uncertainties in these spectral lines is too large to use these results as a direct basis for absolute water vapor calibration (a change in the line strengths by the indicated percent would also achieve consistency). However, the reasonable agreement of these four cases is quite encouraging.

By carefully choosing well suited spectral lines, this technique promises to provide a way to transfer an accurate water vapor calibration based on the AERI on-line data to radiosonde or Raman lidar profiles, as soon as a small number of accurate water vapor observations become available at the SGP. The correct absolute line strengths for a few chosen lines might also be determined using model calculations from profiles calibrated using microwave observations, as suggested by Clough and Brown (1996) who concluded that radiosonde observations are too dry by about 10%. It is curious to note that, if the spectroscopic parameters for the three lines requiring the lowest mixing ratio changes in Figure 6 are

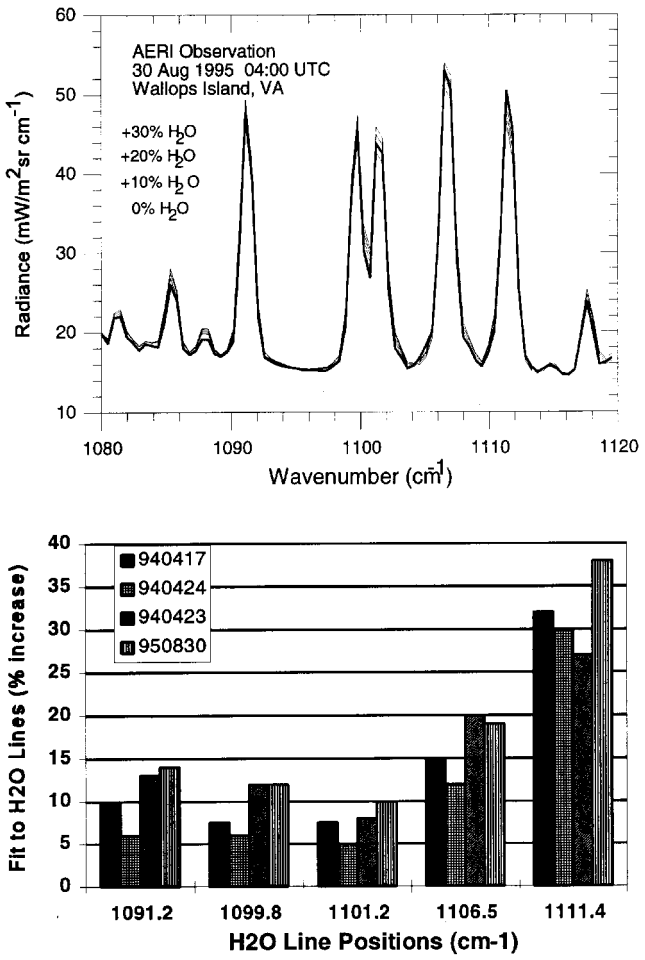

Figure 5. Top: Four models are compared to an AERI observation. The amount of water vapor in each model is scaled and then the continuum shifted to match. The resulting water vapor line strengths are compared to the observation. The best fits for each line are shown in the bottom panel for this case (Wallops Island, Aug 1995), and for three others (CART site, April 1994).

assumed correct, they would also imply that radiosonde observations are about 10% too dry. Ultimately, this process will also lead to identifying and eliminating remaining line strengths errors in the spectroscopic data base.

SGP Aerosol Case Study and Update

Table 1 updates the aerosol table from last year's science team paper (Revercomb et al. 1995). April 26 still stands out as a very strong aerosol case. A dry-line passage occurred

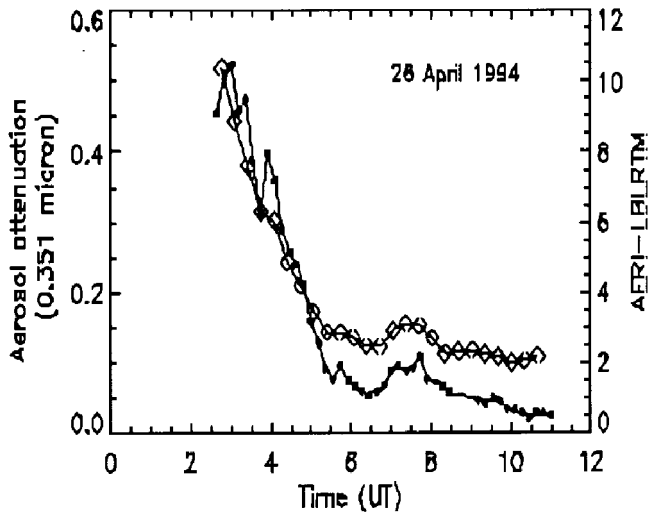

Figure 6. Aerosol evolution on 26 April 1994. The connected diamonds show the Raman-measured attenuation at 0.351 μm (provided by R. Ferrare), and the solid dots are the AERI-LBLRTM radiance difference averaged over 800-1200 cm^{-1}.

at approximately 2 hours UT. Even after the atmosphere dried out and aerosol amounts became low, the AERI-LBLRTM residual still has a measurable signature. Figure 6 shows the time evolution of the aerosols as measured by the Raman lidar and the AERI/LBLRTM residuals. The Raman provides a measure of the aerosol attenuation ($1\text{-}e^{-\delta}$, where δ is optical depth) at 0.351 μm; and AERI-LBLRTM is roughly proportional to aerosol emissivity in the longwave window, here averaged over 8-12 μm (excluding the ozone band). As this figure shows, the longwave and shortwave indicators of aerosol follow each other fairly well during this event.

The longwave spectral signature of the aerosols can be modeled with LOWTRAN subroutines incorporated into the LBLRTM program. Figure 7 shows several of the LOWTRAN aerosol models compared to the AERI/LBLRTM residual at 2.8 hours UT (April 26, 1994). None of the models give a good fit to the spectral shape of this aerosol. The opportunity exists to define an aerosol size distribution and composition that can fit both the shortwave measurements of aerosol amount (at present provided by Raman lidar and the new aerosol measurement facility), and the IR radiative measurements made by AERI.

While Figure 6 indicates that the Raman aerosol optical depths and AERI/LBLRTM residuals follow each other on some occasions, examination of Table 1 shows that this agreement is not universal. The table entries are ordered by increasing precipitable water. Note that the aerosol backscatter ratio (the ratio of aerosol to molecular scattering) follows the precipitable water quite closely. Melfi et al. (1996) show in more detail that the Raman-measured aerosol amounts increase with increasing water vapor amount. In contrast, the AERI/LBLRTM aerosol estimate (Table 1, columns 7 & 8) is not necessarily strongest in high water vapor conditions. On the wettest clear-sky observations, April 23 and 24 1994, the AERI longwave observations show no obvious signature of aerosols. In fact, the AERI-LBLRTM residual is negative on April 24, the wettest case (Figure 4), while a LOWTRAN aerosol model for this date with modest aerosol amount (20 km visibility) implies there would be a measurable signal. It is possible that continuum water vapor opacity errors are masking an aerosol signature. It is also possible that the aerosols behave differently in the longwave in high humidity than the models suggest. This is not surprising since the models use shortwave measurements to derive aerosol composition and size distribution. The longwave measurements should provide further constraints on these aerosol properties.

Summary

The AERI/LBLRTM residuals point to a problem in the consistency of the water vapor measurements made by the BBSS (see also Lesht and Liljegren 1996). However, several other measuring systems at the CART site can be used to correct the radiosonde measurements. These are, the Raman lidar which can check and correct the radiosonde profile; the microwave radiometer (Clough and Brown 1996; Lesht and Liljegren 1996) which can provide an absolute scale factor; the AERI line spectra which also provide a scale factor; and surface and tower observations, to provide checks and to model the lag of the radiosonde response.

When these corrections are made, we will be able to more accurately address the important ARM objectives of improving representations of the water vapor continuum and aerosols.

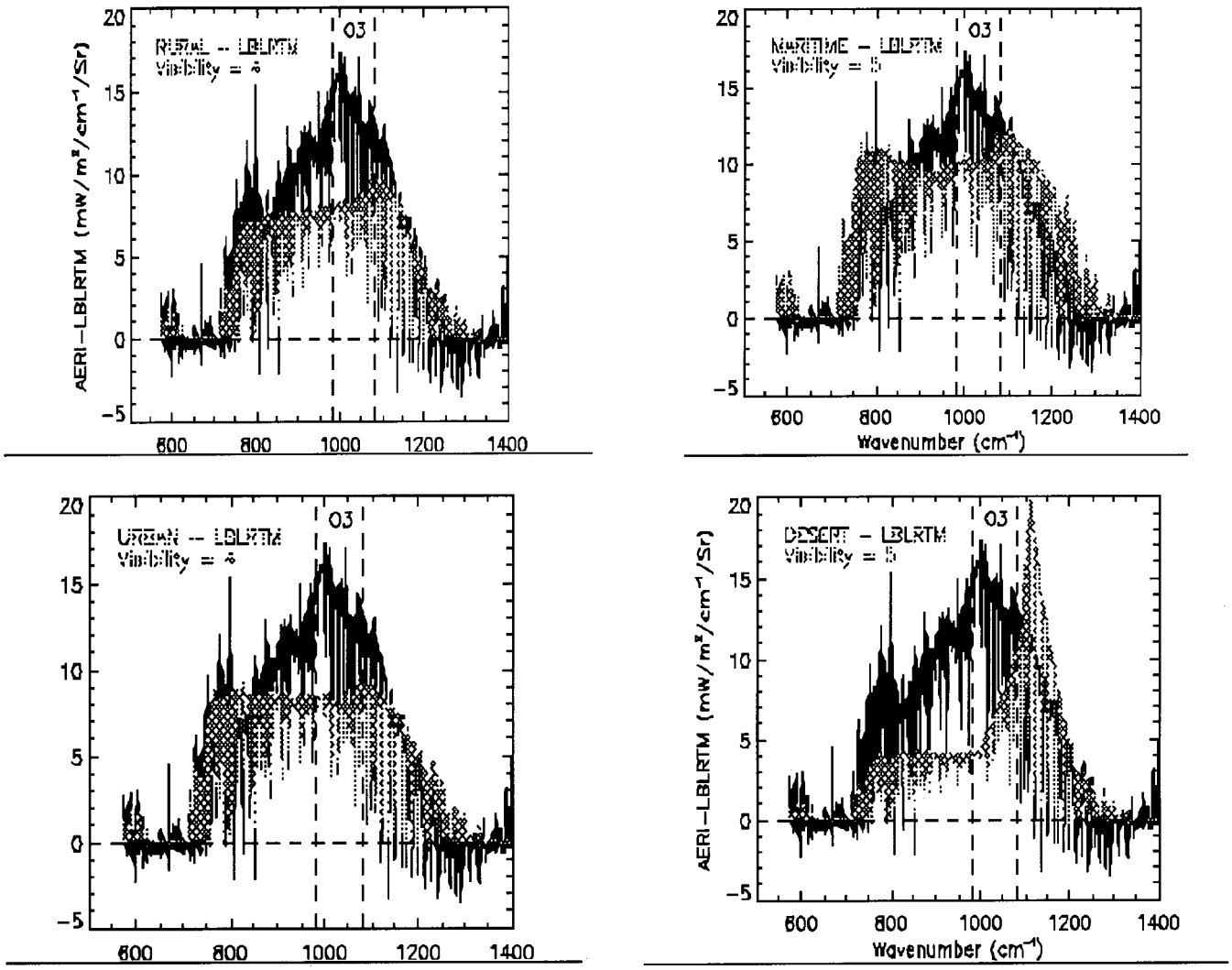

Figure 7. An extremely high aerosol case, on 26 April 1994, at 2.8 hours UT. AERI-LBLRTM residuals reach up to 15 mW/m^2/cm^{-1}/Sr (solid lines). A selection of LOWTRAN aerosol models are plotted in grey. These are plotted as differences between the LBLRTM models with and without aerosols.

References

Clough, S.A., and P. Brown, 1996: The role of microwave radiometric measurements with respect to water vapor and oxygen, this volume.

Clough, S.A., and M.J. Iacono, 1995: Line-by-line calculations of atmospheric fluxes and cooling rates II: Application to carbon dioxide, ozone, methane, nitrous oxide, and the halocarbons, *J. Geophys. Res.*, **100**:16, 519-16,535.

Clough, S.A., C.P. Rinsland, and P.D. Brown, 1995: Retrieval of tropospheric ozone from simulations of nadir spectral radiances as observed from space, *J. Geophys. Res*., **100**:16, 579-16,593.

Clough, S.A., R.D. Worsham, W.L. Smith, H.E. Revercomb, R.O. Knuteson, H.W. Woolf, G.P. Anderson, M.L. Hoke, and F.X. Kneizys, 1989: Validation of FASCODE calculations with HIS spectral radiance measurements, In *IRS ' 8: Current Problems in Atmospheric Radiation*, eds. J. Lenoble and J.E. Geleyn, A. Deepak Publishing, Hampton, Virginia.

Collard, A.D., S.A. Ackerman, W.L. Smith, X. Ma, H.E. Revercomb, R.O. Knuteson, and S.-C. Lee, 1995: Cirrus cloud properties derived from high spectral resolution infrared spectrometry during FIRE II, Part III: Ground-based HIS results, *J. Atmos. Sci.*, **52**:4264-4275.

Ellingson, R.G., S. Shen, and J. Warner, 1995: Calibration of radiation codes used in climate models: Comparison of clear-sky calculations with observations from the spectral radiation experiment and the Atmospheric Radiation Measurement Program, In *Proceedings of the 4th ARM Science Team Meeting*, Charleston, South Carolina, 28 February - 3 March, 1994, p. 47-53.

Feltz, W., B. Smith, B. Howell, and B. Knuteson, 1996: AERI temperature and water vapor retrievals: Improvements using an integrated profile retrieval approach, this volume.

Melfi, S.H., R. Ferrare, K.D. Evans, D. Whiteman, D.O'C. Starr, and R. Ellingson. 1996: Raman lidar and sun photometer measurements of aerosols and water vapor, this volume.

Lesht, B.M., and J.D. Liljegren, 1996: Comparison of precipitable water vapor measurements obtained by microwave radiometry and radiosondes at the southern Great Plains CART site, this volume.

Revercomb, H.E., F.A. Best, R.O. Knuteson, B.A. Whitney, T.P. Dirkx, R.G. Dedecker, R.K. Garcia, P. van Delst, W.L. Smith, and H.B. Howell, 1996: Atmospheric emitted radiance interferometer (AERI), Part I: Status, basic radiometric accuracy, and unexpected errors and solutions, this volume.

Revercomb, H.E., R.O. Knuteson, F.A. Best, T.P. Dirkx, R.G. Dedecker, R. Garcia, H.B. Howell, B.A. Whitney, and W.L. Smith, 1995: Atmospheric emitted radiance interferometer (AERI): Status and the aerosol explanation for extra window region emissions, In *Proceedings of the Fifth Atmospheric Radiation Measurement (ARM) Science Team Meeting*, San Diego, California, March 19-23, 1995, pp. 253-258.

Revercomb, H.E., R.O. Knuteson, W.L. Smith, F.A. Best, R.G. Dedecker, and, H.B. Howell, 1995: Atmospheric emitted radiance interferometer: Status and water vapor continuum results, In *Proceedings of the Fourth Atmospheric Radiation Measurement (ARM) Science Team Meeting*, Charleston, South Carolina, 28 February - 3 March, 1994, p. 259-264.

Smith, W.L., X.L. Ma, S.A. Ackerman, H.E. Revercomb, R.O. Knuteson, 1992: Remote sensing cloud properties from high-spectral resolution infrared observations, *J. Atmos. Sci.*, **50**:1708-1720.